Piezoreflectance in CdTe/(Cd,Zn)Te strained-layer superlattices: Periodicity effect, valence-band offset, and exciton binding energies

J. Calatayud, J. Allègre, and H. Mathieu
Groupe d'Etudes des Semiconducteurs, Université de Montpellier 2, 34095 Montpellier, France

N. Magnéa and H. Mariette
Département de Recherche Fondamentale, Laboratoire de Physique des Semiconducteurs, Centre d'Etudes Nucléaires de Grenoble, Boîte Postale 85X, 38041 Grenoble, France and Laboratoire de Spectrométrie Physique, Université J. Fourier, Grenoble 1, France

(Received 17 July 1992; revised manuscript received 1 December 1992)

We have investigated a series of CdTe/$Cd_{1-x}Zn_xTe$ strained-layer superlattices grown with low Zn concentrations ($x<0.15$). From differential spectroscopy techniques (wavelength modulations and piezomodulations) we identify all heavy-hole and light-hole exciton transitions. Confinement levels have been obtained by envelope-function calculations using a transfer-matrix algorithm. These levels depend not only on the barrier height, the layer thickness, and the material parameters, but also on the growth strain that rules the quadratic deformation in each layer (CdTe or $Cd_{1-x}Zn_xTe$). From the comparison between the calculated transition energies and the experimental values obtained on a series of superlattices, we first deduce a weak chemical valence-band offset between the two materials. We also make an accurate estimation of the binding energies of heavy- and light-hole excitons as a function of the superlattice period, and finally derive the combined conditions of strain and period that control the type (I or II) of a CdTe/(CdZn)Te strained-layer superlattice.

I. INTRODUCTION

The strong lattice mismatch between bulk CdTe and ZnTe (6.4%) makes it difficult to grow heterostructures based on the two binary materials, in spite of the molecular-beam epitaxy facilities. Previous works[1,2] on free-standing CdTe/(Cd,Zn)Te superlattices have shown the feasibility of peseudomorphic growth and evidenced its limit. Indeed Cibert *et al.*[3] have determined that the critical thickness of a strained CdTe layer on a ZnTe substrate was 17 Å and that only strained-layer superlattices (SLS's) with short periods can be grown under elastic conditions. In this work, the problem is drastically reduced by the growth of CdTe and $Cd_{1-x}Zn_xTe$ layers, with Zn composition $x<0.15$. The lattice mismatch is then lower than 1%. In this case, since the CdTe/$Cd_{1-x}Zn_xTe$ superlattice forms a coherently strained system, the in-plane lattice parameter of the entire heterostructure matches with the one of the substrate (or of a buffer layer). This allows us to avoid any relaxation of the strain for the total SLS thicknesses up to about 1 μm.

In such structures, the potential wells that confine the holes are quite shallow, due to the weak discontinuity between the valence bands of CdTe and $Cd_{1-x}Zn_xTe$, whose states originate from p states of the Te anion, common to both materials. A recent work by Tuffigo *et al.*[4] reveals that the valence-band offset (VBO) is strongly strain dependent and that the exact value of the chemical offset (which remains weak), is still unknown. Moreover, depending on the substrate, the strain-induced shift and splitting of the valence bands may induce a reversal of the energy position of the top most valence subbands. Then, the character of the electron-hole transitions can be either type I or type II, depending on the strain-induced alignment of valence bands. We propose a refined insight into the various ingredients that determine the relative energies.

The electron and hole energies have been calculated using a transfer-matrix algorithm.[5] In the case of free-standing SLS's and assuming a zero valence-band offset, the calculation is straightforward and predicts electrons and heavy holes preferentially confined in CdTe layers; on the contrary, the light holes are confined in $Cd_{1-x}Zn_xTe$ layers. In this work, our spectroscopic results have been interpreted by taking into account (i) a nonzero valence-band offset, (ii) the influence of the strain provoked by the substrate, and (iii) the variation of the exciton binding energy (EBE).

This paper is organized as follows. In Sec. II we present the theoretical approach that was applied to strained heterostructures. In Sec. III piezomodulation techniques are used to assign in terms of light-hole or heavy-hole excitons the optical transitions observed by reflectivity. Finally, in Sec. IV we interpret our results and deduce the VBO and the variation of exciton binding energies as a function of the SLS period. This allows us to derive the combined conditions of strain and period which determine the type (I or II) of the fundamental gap of a CdTe/(Cd,Zn)Te SLS.

II. BASIC FORMALISM

Two-dimensional heterostructures, such as quantum wells, multiple quantum wells, and SLS's, present a step-

like potential profile. We use the envelope-function formalism of Bastard[6] for states near the center of the Brillouin zone, for which the upper valence bands can be considered decoupled. The energy and envelope function $\psi(z)$ of a given type of carrier are obtained by the resolution of the effective-mass equation:

$$\left[-\frac{\hbar^2}{2}\frac{\partial}{\partial z}\frac{1}{m^*(z)}\frac{\partial}{\partial z}+V(z)\right]\psi(z)=E\psi(z)\ , \tag{1}$$

where $m^*(z)$ is the effective mass of the carrier and $V(z)$ the steplike potential energy for this carrier. The latter is obtained from the alignment of band extrema in both materials, which results from (i) the so-called chemical VBO and (ii) the strain-induced energy shifts of the various extrema. We have used a transfer-matrix algorithm[5] in which Bastard's continuity conditions are expressed in a matricial way. The set of relevant parameters used to account for CdTe and $Cd_{1-x}Zn_xTe$ band structures and for strain effects is presented below.

At $T=2$ K, the energy gap, the electron effective mass, and the valence-band parameters of the alloy have been taken as[7,8]

$$E_g(x)=1.606(1-x)+2.394x-0.26x(1-x)\ \text{eV}\ , \tag{2}$$

$$\frac{m_e^*(x)}{m_0}=0.099+0.017x\ , \tag{3}$$

$$\gamma_1(x)=4.11-0.04x\ , \tag{4}$$

$$\gamma_2(x)=1.08-0.3x\ . \tag{5}$$

The lattice parameter of $Cd_{1-x}Zn_xTe$ was obtained from[9]

$$a(Cd_{1-x}Zn_xTe)=6.481-0.3773x\ \text{Å}\ . \tag{6}$$

Since our SLS's are generally coherently grown on a (001) $Cd_{1-y}Zn_yTe$ substrate with $0<y<x$, the CdTe layers are biaxially compressed and the $Cd_{1-x}Zn_xTe$ layers are biaxially stretched, the plane perpendicular to the growth direction. In this case, the crystalline structure of the materials becomes tetragonal with a common lattice parameter a_s in the plane of the layers, and different lattice parameters $a_\perp(i)$ along the growth direction of the SLS.

$$a_\perp(i)=a_i[1+2(S_{12}X_i)]$$
$$\text{(compound } i\text{: CdTe, CdZnTe)}\ . \tag{7}$$

In other words, each compound (i) sustains an internal stress X_i given by

$$X_i=\frac{a_s-a_i}{a_iS_i}\ , \tag{8}$$

where a_s and a_i are the lattice parameters of the substrate and compound i, respectively, and $S_i=(S_{11}+S_{12})_i$, where S_{11} and S_{12} are the elastic compliance constants. Several values for these constants are presented in the literature.[10–14] For CdTe, we took the values obtained experimentally at $T=4$ K by Greenough and Palmer.[13] Concerning ZnTe, we have used the experimental values of Ref. 14.

The stress-induced energy shifts of the bands can be calculated using the proper set of deformation potentials. Recently, Zigone *et al.*[15] and Prakash *et al.*[16] performed low-temperature experiments under hydrostatic pressure. They showed that, for weak hydrostatic pressures (which is the case in our heterostructures), an appropriate value of the band-gap hydrostatic coefficient is $dE_g/dP=-7.6$ meV/kbar. The corresponding hydrostatic deformation potential is $a=-3.42$ eV. We have obtained the repartition of this potential between the conduction and valence bands from the ratio $a_c/a_v=-1.9$ given in Ref. 17. Concerning the tetragonal deformation potential, the value $b=-0.98$ eV is obtained from the ratio $b/a=0.285$, determined on CdTe epilayers by Allègre *et al.*[18] Concerning ZnTe, the deformation-potential values are given in Refs. 19 and 20. They are not discussed here because their influence on the deformation potentials of $Cd_{1-x}Zn_xTe$ ($x\leq 0.15$) is rather weak.

We can thus estimate the interface strain effects on the band structure of bulk materials.[21,22] The energy shifts of the lowest conduction band and upmost valence bands are written as

$$\Delta E_{c_i}=2a_{c_i}(S_{11}+2S_{12})_iX_i\ , \tag{9}$$

$$\Delta E_{\mathrm{hh}_i}=[2a_{v_i}(S_{11}+2S_{12})_i+b_i(S_{11}-S_{12})_i]X_i\ , \tag{10}$$

$$\Delta_{E_{\mathrm{lh}_i}}=[2a_{v_i}(S_{11}+2S_{12})_i-b_i(S_{11}-S_{12})_i]X_i\ . \tag{11}$$

The main effect is the stress-induced splitting of the Γ_8 fourfold valence band, and the behavior of the structure is very different depending on whether the heavy- or light-hole band (denoted by hh and lh, respectively) is involved in the fundamental transition. For convenience, all computational parameters have been listed in Table I.

III. EXPERIMENT

All $CdTe/Cd_{1-x}Zn_xTe$ SLS's have been grown by molecular-beam epitaxy on (001)-oriented $Cd_{1-y}Zn_yTe$ substrates with $y\sim x/2$. Reflection high-energy electron diffraction provided the means to optimize the two-dimensional layer-by-layer growth of CdTe and $Cd_{1-x}Zn_xTe$ and to measure *in situ* the layer thickness to one monolayer accuracy. The alloy composition x together with the period of the SLS were precisely determined from x-ray diffraction.[23,24] In order to perform a coherent elastic growth of our layers, we used the strain-symmetrization procedure developed for Si/Ge systems:[25] the thicknesses of CdTe and $Cd_{1-x}Zn_xTe$ were kept

TABLE I. Basic parameters used in the electronic structure calculation. The values for $Cd_{1-x}Zn_xTe$ materials are obtained by linear interpolation between CdTe and ZnTe values.

	CdTe	ZnTe
a_c (eV)	−2.25	−5.19 (Ref. 19)
a_v (eV)	1.17	0.34 (Ref. 19)
b (eV)	−0.98	−1.20 (Ref. 20)
S_{11} (kbar^{-1})	4.16×10^{-3} (Ref. 13)	2.38×10^{-3} (Ref. 14)
S_{12} (kbar^{-1})	-1.71×10^{-3} (Ref. 13)	-0.857×10^{-3} (Ref. 14)

equal. This leads to a situation very close to the one of a free-standing superlattice. The biaxial strain is equally shared between both materials. CdTe layers undergo a compression perpendicular to the growth axis, while $Cd_{1-x}Zn_xTe$ layers sustain a dilatation. This strain symmetrization was applied to all the samples except samples *C* and *D*, which were grown on CdTe and in which all the strain was supported by the only $Cd_{1-x}Zn_xTe$ layers. More technical details about the growth of $CdTe/Cd_{1-x}Zn_xTe$ SLS have been reported in Refs. 26 and 27.

The amount of zinc in $Cd_{1-x}Zn_xTe$ ranges from 6 to 12%; the potential barrier between CdTe and $Cd_{1-x}Zn_xTe$ ranges from 40 to 80 meV. The repartition of this barrier between conduction and valence bands is one of the points we intend to address.

Figure 1 presents typical low-temperature reflectivity spectra, collected under normal incidence for eight samples with increasing periods, ranging from 65 to 400 Å (curves *A*–*H*). The energy range spans the interval between the gaps of the two materials (CdTe and $Cd_{1-x}Zn_xTe$, respectively), and all spectra reveal different series of features.

(i) Features from the SLS's; they are labeled e_ih_j and

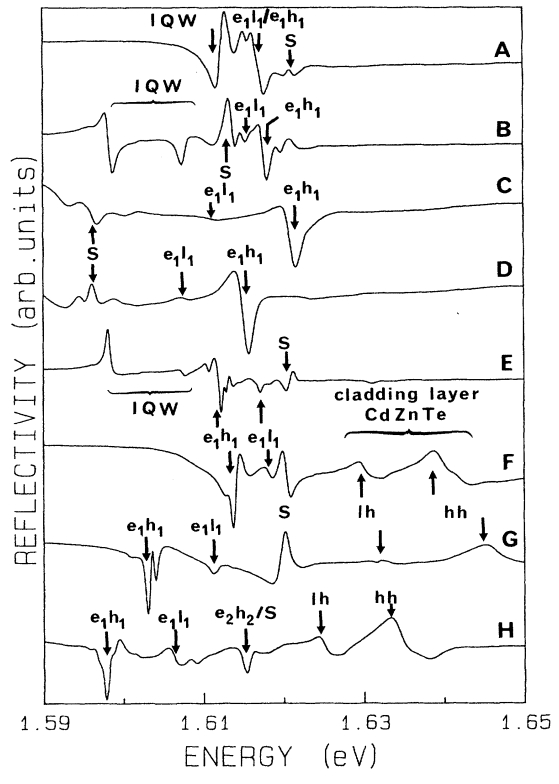

FIG. 1. Direct reflectivity spectra of strained-layer $CdTe/Cd_{1-x}Zn_xTe$ superlattices for different nominal periods: *A* and *B*, 35 Å/35 Å; *C*, *D*, and *E*, 70 Å/70 Å; *F*, 70 Å/140 Å; *G*, 130 Å/130 Å; *H*, 200 Å/200 Å. *C* and *D* samples are grown on CdTe buffer layers. In samples *A*, *B*, and *E*, the features, at low energy are due to an IQW. In samples *F*, *G*, and *H*, a bulk $Cd_{1-x}Zn_xTe$ capping layer has been included: the light-hole (lh) and heavy-hole (hh) splitting appears at high energy.

e_il_j. The most intense is always the direct heavy-hole ground-state exciton transition e_1h_1; we have only labeled this transition and the light-hole one e_1l_1. For clarity, the calculated band-to-band transitions will be denoted in capitals: E_iH_j, E_iL_j.

(ii) The feature from the substrate or buffer layer, labeled *S*, is always visible and allows us to check the substrate composition exactly and thus to determine the correct in-plane lattice parameter a_s.

(iii) In some cases (samples *A*, *B*, and *E*), a CdTe isolated quantum well (IQW), wider than the other CdTe layers of the SLS, is present. This results in additional features at low energy.

(iv) Finally, when a $Cd_{1-x}Zn_xTe$ capping layer was grown (samples *F*, *G*, and *H*), features from this bulk alloy appeared on the high-energy side. These features labeled hh and lh show a typical light-hole–to–heavy-hole splitting. This is a complementary means to measure *x* in the barrier layers ($Cd_{1-x}Zn_xTe$) and to know the real strain borne by the heterostructure.

Note that sample *F* is a SLS with asymmetric layer thicknesses: $d[CdTe] \sim \frac{1}{2}d[(Cd,Zn)Te]$. This results in the fact that the confinement levels and the transition energies are close to the levels in a sample with a shorter period.

All the transitions have been identified in terms of electron-light-hole and electron-heavy-hole excitons from piezomodulation experiments (see below). Figure 1 shows that the energy of the heavy-hole ground-state exciton e_1h_1 increases when the period increases. Also notice the relative position of the light-hole exciton $[e_1l_1(l)]$ regarding the heavy-hole one $[e_1h_1(h)]$, which determines the type of the structure. We have the order *h*,*l*,*S* or *S*,*l*,*h* depending on the energy of the substrate feature (*S*) which is related to the common in-plane lattice parameter.

Typical spectra are shown in Figs. 2 and 3 for samples *B* and *E*, respectively. These samples are representative of the two different situations which can be met: (i) type II, with the light-hole level as the ground state and (ii) type I, with the heavy-hole level as the ground state. In both cases, the SLS has a total thickness equal to 1 μm and includes a 210 Å-wide CdTe extended well at a depth of about $\frac{1}{4}$ of the total length of the SLS. The Zn contents of the $Cd_{1-x}Zn_xTe$ barrier were, respectively, 8.7% and 10.3%. They were grown on $Cd_{1-y}Zn_yTe$ substrates with $y = 3.45\%$ and 4.5% respectively, which is slightly less than the composition of the alloy $Cd_{1-x/2}Zn_{x/2}Te$, globally equivalent to the SLS. This results in slightly increasing the strain into the barrier, with respect to the symmetric "free-standing" situation. The main difference between these two samples lies in their periods: 67 Å (32 Å/35 Å) for sample *B*, 144 Å (71 Å/73 Å) for sample *E*.

In Figs. 2 and 3, we compare the direct reflectivity spectrum (curve *R*) with the wavelength modulated (WMR) and piezomodulated (PMR) reflectivity spectra. In all spectra, we find (i) features due to the 210-Å-wide IQW, labeled 1, 2, 3, and 4; (ii) features due to the superlattice, labeled 5, 6, 7, and 8, and (iii) the feature due to the substrate, labeled *S*. Note that, in Fig. 2, transitions

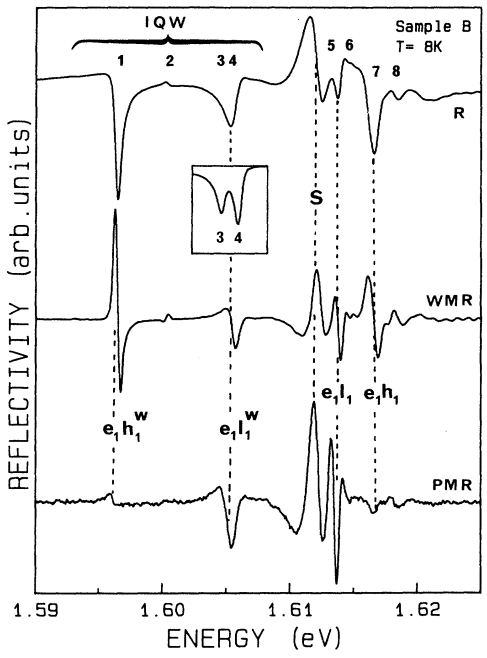

FIG. 2. Reflectivity spectrum (R), and PMR spectra of a short-period SLS (sample B). The spectrum in the inset is obtained by applying a tensile biaxial strain of ~ 200 bars, and reveals that the features 3 [$e_1h_1(N=3)$] and 4 [e_1l_1] are degenerate. The latter has been identified by piezomodulation (not represented).

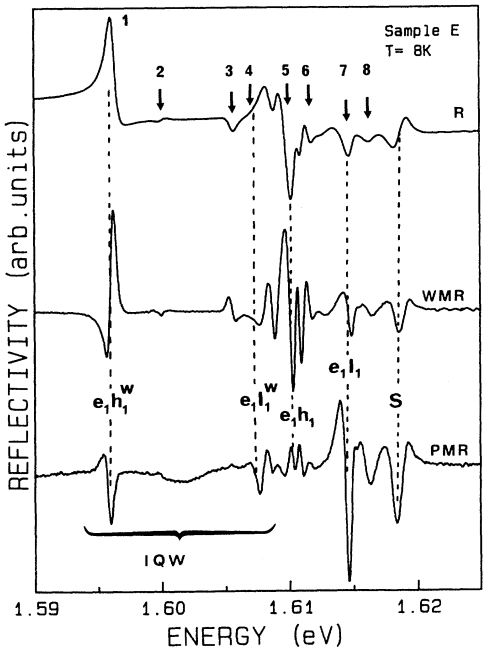

FIG. 3. Reflectivity spectrum (R), WMR, and PMR spectra of a SLS (sample E) with an intermediate period.

3 and 4 are superimposed. The application of an external biaxial strain allows us to distinguish between them (see the inset in Fig. 2). In previous papers[18,22] we have shown that the amplitude ratio of the PMR vs WMR spectra is small for a transition involving a heavy-hole level and large for a light-hole level. We thus identify the transitions as follows.

Among the low-energy series of structures (1,2,3,4), transitions 1, 2, and 3 correspond to the so-called center-of-mass quantization of the heavy-hole exciton ($e_1h_1^w$, $N=1,2,3$) inside the 210-Å-wide CdTe well. Indeed, recent works[4] showed that, for wells wider than 200 Å, the energy levels of the confined exciton should be calculated as the quantization of the exciton polariton as a whole. Only for such wide wells, this approach is more accurate than the usual calculation of the binding energy of independently confined electrons and holes, which remains relevant for our SLS's.

The fourth line (4) is due to the ground-state light-hole exciton transition $e_1l_1^w$. This is revealed by the exhausted piezomodulation response (curve PMR). It is exceptional to clearly observe such signature of a type-II transition. This is due to the fact that the barriers are superlattices: the light holes are better confined and the E_1L_1 transition has a nonvanishing oscillator strength.

The $Cd_{1-y}Zn_yTe$ substrate is not strained so that its ground-state transition is degenerate and the modulation is a mixing of both heavy- and light-hole terms. Feature S, which only depends on the composition y, takes place at lower energy in sample B ($y=3.45\%$) than in sample E ($y=4.46\%$). Next, concerning the four SLS features (labeled 5,6,7,8) the main experimental result is the piezomodulation behavior: features 5 and 6 are quenched in sample E (curve PMR, Fig. 3) and exhausted in sample B (curve PMR, Fig. 2). In other words, the ground state involves a light-hole type-II transition e_1l_1 for sample B (Fig. 2) and a heavy-hole type-I transition e_1h_1 for sample E (Fig. 3). At higher energy, the contrary occurs, the features 7 and 8 are heavy-hole-like for sample B and light-hole-like for sample E. In Table II, we list all the results obtained on both samples. (Note that transitions 6 and 8 are not strictly identified; they may be due to monolayer thickness fluctuation.)

We took advantage of piezomodulated reflectivity spectra to identify e_1h_1 and e_1l_1 transitions in each of our samples. The experimentally measured energies have been reported in Table III.

We remark that samples C and D were grown on a 2-μm-thick CdTe buffer layer. It follows that the strain is mainly localized in the $Cd_{1-x}Zn_xTe$ layers, since the CdTe layers are almost not disturbed. Thus, the light-hole well localized in the $Cd_{1-x}Zn_xTe$ is clearly featured and it is not surprising to find the e_1l_1 type-II exciton as the ground state of the SLS.

Finally, notice that in all the cases where a buffer layer exists, the fit of the calculated values to the experimental ones is not perfect. The relaxation of the buffer layer perturbs the (001) cylindric symmetry and the strain effect is probably miswritten in our formalism. As an evidence for this, curves C and D in Fig. 1 shows a light-hole–to–heavy-hole splitting of 3 meV for feature S,

TABLE II. Identification of the experimental features shown in Fig. 2 for sample *B* and in Fig. 3 for sample *E*.

Feature		Sample *E* Energy (eV)	Piezoresult	Transition	Sample *B* Energy (eV)	Piezoresult	Transition
QW	1	1.597	heavy	$(e1h1)N=1$	1.596	heavy	$(e1h1)N=1$
	2	1.600	heavy	$(e1h1)N=2$	1.600	heavy	$(e1h1)N=2$
	3	1.607	heavy	$(e1h1)N=3$	1.605	light	$e1h1$
	4	1.611	light	$e1l1$	1.605	light	$e1l1$
Substrate *S*		1.620	mixed	gap ($y=4.45\%$)	1.614	mixed	gap ($y=3.46\%$)
SL	5	1.612	heavy	$e1h1$	1.616	light	$e1l1$
	6	1.614	heavy	?	1.617	light	?
	7	1.617	light	$e1l1$	1.619	heavy	$e1h1$
	8	1.618	light	?	1.620	heavy	?

characteristic of the CdTe buffer layer. This means that the buffer layer contains a residual strain, which affects the lattice parameter. Reflectivity experiments show that type-II superlattices are obtained when a sufficient strain exists in the $Cd_{1-x}Zn_xTe$ layers.

IV. DISCUSSION

In Table III, we list all the basic characteristics of our heterostructures. The electronic states have been calculated as a function of the chemical offset for four samples (*B*,*E*,*G*,*H*); the corresponding transition energies are displayed in Figs. 4(a)–4(d), respectively. The heavy-hole transitions are shown by a full line and light-hole transitions by a dashed line. Some curves are interrupted when one of the two energy levels (electron or hole) reaches the edge of the well: the corresponding transitions cease to be strongly allowed. The vertical line, at about $Q_V=0.19$ separates the type-I and type-II regions, for heavy holes. The light holes remain type II down to $Q_V=-0.30$. Finally the experimental values e_1h_1 and e_1l_1 are shown by full and dashed bold horizontal lines.

A. Exciton binding energy

In the case of short-period SLS's [Fig. 4(a)], the confinement energy of free carriers is large and only one subband of bound states exists. The curves are limited to ground-state transitions: E_1H_1 and E_1L_1. We note that both transitions are very weakly affected by the chemical offset. This is not surprising since, in that case, we are in the presence of minibands rather than spatially confined states. The curves do not bring out any significant information about the offset value, but are relevant for extracting the EBE's, whatever the valence-band offset. We obtain $E_1H_1-e_1h_1=11.5\pm0.5$ meV and $E_1L_1-e_1l_1=10.5\pm0.5$ meV. This confirms the fact that when the period goes towards 0, the symmetric superlattice tends to behave like the equivalent $Cd_{1-x/2}Zn_{x/2}Te$ alloy, for which the exciton has a characteristic 3D value (11 meV).

TABLE III. Characteristics of the studied $CdTe/Cd_{1-x}Zn_xTe$ superlattices.

Nominal period	CdTe/CdZnTe thicknesses (Å)	*x* (%) Zn barriers	*y* (%) Zn substrate	Additional features	*E*1*H*1 and *E*1*L*1 (calc.) (meV)	*e*1*h*1 and *e*1*l*1 (expt.) (meV)
Sample *A*	34/32	8.8	4.6	66-Å	1629	1618
35/35 Å				isolated QW	1629	1618
Sample *B*	32/35	8.7	3.45	210-Å	1630	1618
35/35 Å				isolated QW	1626	1616
Sample *C*	65/64	14	CdTe	131-Å	1635	1621
70/70 Å			buffer	cladding layer	1614	1611
Sample *D*			CdTe	150-Å	1629	1615
70/70 Å	65/67	10	buffer	cladding layer	1615	1608
Sample *E*				210-Å	1627	1612
70/70 Å	71/73	10.3	4.5	isolated QW	1623	1617
Sample *F*					1627	1613
70/140 Å	71/138	8.25	4.55		1623	1618
Sample *G*				244-Å	1618	1603
130/130 Å	128/126	9	4.45	cladding layer	1614	1611
Sample *H*				290-Å	1612	1597
200/200 Å	197/197	7.5	4	cladding layer	1608	1607

It is strictly the case for sample A. For sample B, which has the same period as sample A, the transfer-matrix algorithm calculation clearly provides a type-II light-hole ground-state [Fig. 4(a)], because the Zn composition of the substrate is lower than the one of the equivalent alloy. Experimentally we also find a light-hole, type-II excitonic ground state, since the weak discrepancy between light-hole and heavy-hole EBE's forbids us to change the type-I character into type-II character.

On the contrary, when the period increases, the overlap integral of the envelope functions of electrons and light holes fastly decreases[4] from 0.9, for the 35 Å/35 Å SLS (sample A) to 0.05, for the 70 Å/70 Å one (sample E). Starting from the usual intuition that the fundamental exciton state is a 1s-like state, the corresponding EBE then tends towards zero due to the increasing separation between electrons and holes. We believe that this is not exact and that in such a type-II configuration, the fundamental exciton loses its purely s-orbital character and becomes some sort of mixing between s-like and p_z-like orbitals. For very wide periods, the asymptotic limit, which could be similar to a $2p_z$-like interface exciton, with an EBE equal to $0.25R_{3D}$.[28] Therefore, the light-hole EBE fades from 11 meV (equivalent alloy) to a value close to 2.75 meV. We have tried to observe the 2s lh exciton state in order to deduce the value of the binding energy, but the weak oscillator stress and the low expected shift of the transition did not allow us to observe the state. We thus arbitrarily chose to put the asymptotic value for the light-hole Rydberg close to the 2p-like exciton value: we took a value of 3 meV, in reasonable agreement with recent theoretical calculations.[29]

For transitions involving electrons and heavy holes, both particles are strongly localized in the same material (CdTe). The oscillator strength of the transition e_1h_1 and the heavy-hole EBE increase together with the period,

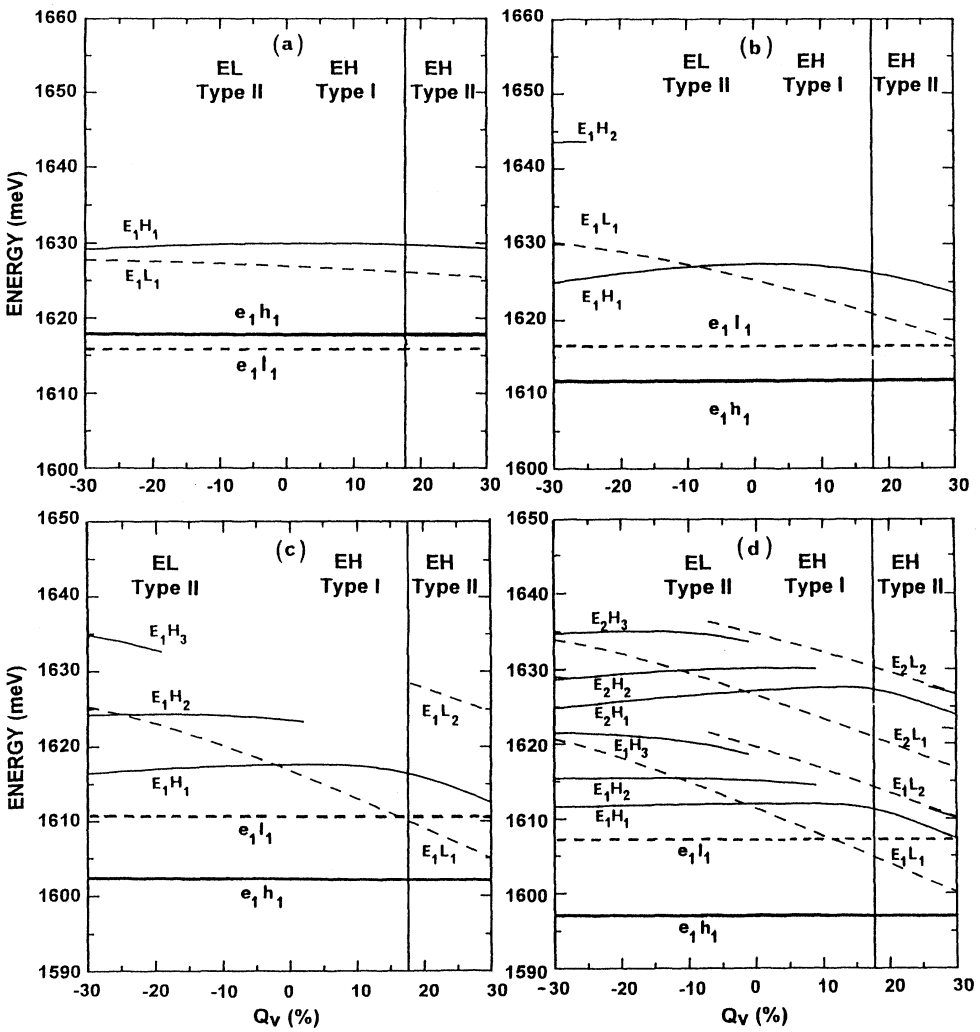

FIG. 4. Calculated transition energies as a function of the chemical VBO ratio Q_V for four cases: (a) sample B (35 Å/35 Å), (b) sample E (70 Å/70 Å), (c) sample G (130 Å/130 Å), and (d) sample H (200 Å/200 Å). E_nH_n full line; E_nL_n, dashed line; and the experimental excitonic ground-state levels (e_1h_1 and e_1l_1), full and dashed bold lines.

going towards the situation of an exciton in a single quantum well. For instance, in a $CdTe/Cd_{0.92}Zn_{0.08}Te$ quantum well the highest binding energy found, in this case, is 25 meV for a 50-Å thick well.[30] In the case of $CdTe/Cd_{1-x}Zn_xTe$ SLS's with equal well and barrier thicknesses, the highest EBE is obtained for the smallest barrier thickness for which the quantum coupling between CdTe successive wells vanishes. Beyond this thickness, the energy minibands of the carriers transform into discrete levels. This thickness is approximately 160 Å. For a well width of 160 Å an EBE of about 15 meV is found.[30]

When the SLS period increases, we thus expect a variation of the exciton binding energy in between 11 and 15 meV for e_1h_1 transitions and from 11 meV to ~3 meV for e_1l_1 transitions. In other words, Q_V values leading to Rydberg values outside these limits will be rejected.

B. Chemical valence-band offset

For SLS periods greater than 30 monolayers (~50 Å/50 Å) all the excitonic fundamental gaps identified on reflectivity spectra are type I (curves $E-H$ in Fig. 1). On the opposite, samples C and D remain type II since they were grown on a CdTe buffer layer: the lattice mismatch strain only affects the $Cd_{1-x}Zn_xTe$ layers and consequently shifts the light-hole level at lower energy than the heavy-hole ground-state, which remains localized within unstrained CdTe layers. This case was studied in Ref. 4.

Figures 4(b)–4(d) respectively, referring to samples E (70 Å/70 Å), G (130 Å/130 Å) and H (200 Å/200 Å), clearly show that the E_1L_1 transition is very sensitive to any variation of the valence-band offset. On the contrary the E_1H_1 transition remains almost independent on this parameter; in fact, the only modified value is the well depth which plays a secondary role on the carrier confinement and thus, on the transition energy value. The different sensitivities of the EL and EH to the offset variation is full of interest in the case of large periods. For instance, in Fig. 4(d), sample H (200 Å/200 Å) should be considered as a multiple quantum well, with low interwell coupling, rather than a superlattice. Here, the transition e_1l_1 is clearly type II and the light-hole EBE is slightly larger than the value for the $2p$-like interface exciton, as explained above. If we assume that the EBE is equal to E_R ($2p$ exciton)=3 meV, and if we identify the difference between E_1L_1 and e_1l_1 to this energy, the analysis of Fig. 4 demonstrates that the highest possible value for the VBO is 1%. In fact, the EBE is most probably closer to 4 meV, which leads to a VBO of −2%.

For every sample, we made such an interpretation of the energy diagrams, accounting for the increase of the heavy-hole EBE $E_R(e_1h_1)$ and the decrease of the light-hole EBE $E_R(e_1l_1)$ as a function of the period. This is particularly significant for samples with large periods. For a given value of Q_V, we could plot the empirical EBE values $E_R(e_1h_1)=(E_1H_1-e_1h_1)$ and $E_R(e_1l_1)=(E_1L_1-e_1l_1)$, versus the period. Such values have been reported with rectangles and triangles, respectively, in Fig. 5, for $Q_V=-2\%$ which is the value which provides such

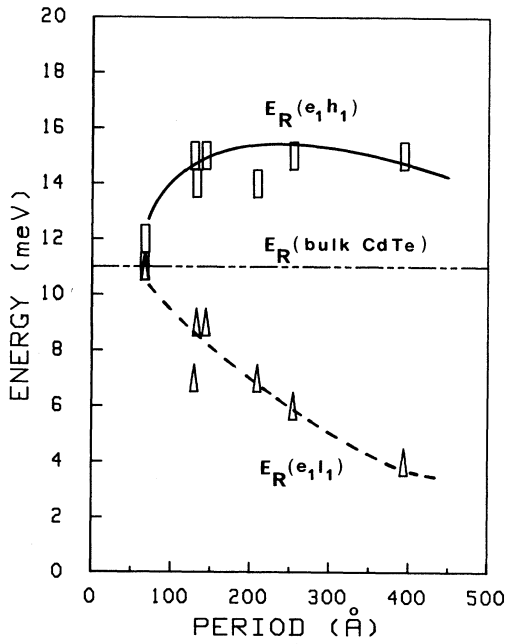

FIG. 5. Exciton binding energies of the ground-state transitions E_1H_1 (rectangles) and E_1H_1 (triangles) for the series of $CdTe/Cd_{1-x}Zn_xTe$ SLS's.

smooth variations and the best overall agreement with existing theoretical models. In some cases, where buffer layers have been used, the result slightly stays away from the average behavior. In fact, we believe that this is due to a nonbiaxial relaxation of the strain in some buffer layers, which makes the calculation of EL and EH erroneous. Sample C is one of these cases. Through the experimental points, we have drawn lines. These lines should be a good empirical determination of the variation of $E_R(e_1h_1)$ and $E_R(e_1l_1)$ as a function of the period.

In summary, we have studied several samples, of well-distributed periods. We have analyzed our results by varying the VBO and by verifying the compacity of the variations of the obtained EBE's. The best results correspond to $Q_V=-0.02\pm0.03$. This value is intermediate between the ones found first by Deleporte *et al.*[31] ($Q_V<-15\%$) for CdTe/(CdZn)Te QW separate confinement heterostructures and second by Peyla *et al.*[29] ($Q_V=3\%$) on the same CdTe/(CdZn)Te SLS's samples as ours. If one uses the repartition of deformation potentials $a_c/a_v=-7.2$ proposed by Van de Walle,[32] we obtain 3% for the VBO. This value agrees well with the calculations of Ref. 29. We remark that both VBO ratio values (−2% and 3%) are very close to zero and the corresponding offset variations do not exceed 2 meV in these Zn-poor heterostructures.

C. Type-I or type-II character

The calculated energies of the E_1H_1 and E_1L_1 transitions versus the period are reported in Fig. 6(a), for a free-standing SLS. The strain distribution in CdTe and $Cd_{1-x}Zn_xTe$ layers is such that the light-hole level de-

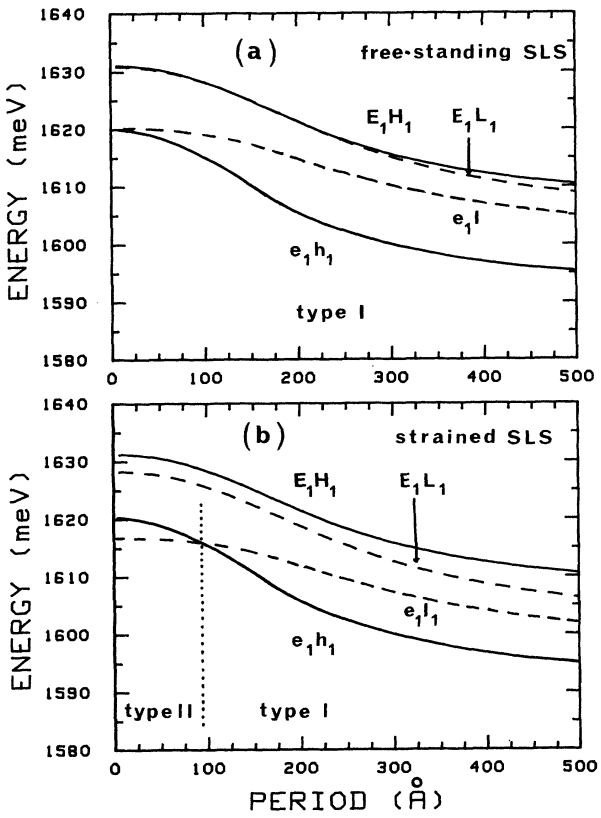

FIG. 6. Band-to-band and excitonic ground-state energies as a function of the period parameter to a $CdTe/Cd_{0.91}Zn_{0.09}$ SLS: (a) in a free standing case (growth on a $Cd_{0.955}Zn_{0.045}Te$ substrate); (b) with a residual strain imposed by the $Cd_{0.965}Zn_{0.035}Te$ substrate.

creases from the degenerate value (obtained for the equivalent bulk alloy $Cd_{1-x/2}Zn_{x/2}Te$) slightly faster than the heavy-hole one, and gives $E_1H_1 > E_1L_1$, but the VBO value around -2% nearly cancels this effect. Now, in this case, the observed excitonic gaps are such that $e_1h_1 < e_1l_1$, whatever the period because the splitting between the heavy- and light-hole EBE's is larger than the one of band-to-band transitions. This is shown in Fig. 6(a) for a sample with the $CdTe/Cd_{0.91}Zn_{0.09}Te$ SLS and a $Cd_{0.955}Zn_{0.045}Te$ substrate.

Generally, the $Cd_{1-y}Zn_yTe$ substrate lattice parameter is different from the one of the $Cd_{1-x/2}Zn_{x/2}Te$ equivalent alloy. Without a total relaxation, the SLS sustains an interface strain. The main effect of the energy splitting of the valence band acts on the light-hole subband. The heavy-hole subband stands by. In other words, the curve E_1L_1 is translated proportionally to the strain. The really interesting case is one for which the E_1L_1 energy decreases ($y < x/2$). Figure 6(b) shows the ground-state transitions of $CdTe/Cd_{0.01}Zn_{0.09}Te$ SLS strained by a $Cd_{0.965}Zn_{0.035}Te$ substrate (case of sample B). We see that E_1L_1 is clearly lower than E_1H_1. The excitonic gaps are such that, now, $e_1l_1 < e_1h_1$ for short periods, the SLS ground-state level is light and type II. For a higher period, we find again a type-I SLS; this is due to the fast decrease of the light-hole EBE. Thus, the choice of the period can be decisive for controlling the type of the ground-state level for a $CdTe/Cd_{1-x}Zn_xTe$ SLS. Note finally that, if the VBO was much lower than -2%, sample B could not be a type-II SLS, as unambiguously observed.

V. CONCLUSION

Piezoreflectance allowed us to assign to light-hole and heavy-hole excitons the fundamental energy gaps of a series of $CdTe/Cd_{1-x}Zn_xTe$ strained-layer superlattices. We have observed that the heavy- and light-hole excitons were degenerate in short-period SLS's. We have compared the calculated band-to-band transition energies to the measured ones, for different values of the valence-band offset. This allowed us to follow the influence of increasing the period on the heavy- and light-hole exciton binding energies, high enough to reach the values found in decoupling quantum wells. Our results, as a whole, have shown a maximum compatibility with a weak valence-band offset such as $Q_V \sim -2\%$ of the band-gap discontinuity. Finally we have determined the combined conditions of strain and period necessary to obtain a type-II SLS. These conditions are strongly dependent on the strength of Coulombic effects.

ACKNOWLEDGMENTS

The Groupe d'Etudes des Semiconducteurs and the Laboratoire de Spectrométrie Physique are Unité associée au Centre National de la Recherche Scientifique.

[1]E. Monfroy, S. Sivananthan, Y. Chu, J. P. Faurie, R. D. Knox, and J. L. Standenmann, Appl. Phys. Lett. **49**, 153 (1986).
[2]H. Mathieu, A. Chatt, J. Allègre, and J. P. Faurie, Phys. Rev. B **41**, 6082 (1990), and references cited therein.
[3]J. Cibert, Y. Gobil, Le Si Dang, S. Tatarenko, G. Feuillet, P. H. Jouneau, and K. Saminadayar, Appl. Phys. Lett. **56**, 292 (1990).
[4]H. Tuffigo, N. Magnea, H. Mariette, A. Wasiela, and Y. Merle d'Aubigné, Phys. Rev. B **43**, 14629 (1991).
[5]B. Jonsson and S. T. Eng, IEEE J. Quantum Electron. **QE-26**, 2025 (1990).
[6]G. Bastard, Phys. Rev. B **24**, 5693 (1981).
[7]*Numerical Data and Fractional Relationships in Science and Technology,* edited by O. Madelung, Landolt-Börnstein, New Series, Group III, Vol. 17B (Springer-Verlag, Berlin, 1982).
[8]C. Neumann, A. Nothe, and N. O. Lipari, Phys. Rev. B **37**, 922 (1988).
[9]D. J. Olego, J. Petruzello, S. K. Ghandi, N. R. Tadxar, and I. B. Bhat, Appl. Phys. Lett. **51**, 127 (1987).
[10]D. Berlincourt, H. Jaffe, and L. R. Shiosawa, Phys. Rev. **129**, 1009 (1963).
[11]H. J. Mc Skimin and D. J. Thomas, J. Appl. Phys. **33**, 56 (1962).
[12]Y. K. Vekilov and A. P. Rusakov, Fiz. Tverd. Tela (Leningrad) **13**, 1157 (1971) [Sov. Phys. Solid State **13**, 956 (1971)].
[13]R. D. Greenough and S. B. Palmer, J. Phys. D **6**, 587 (1973).

[14]W. Wardzynski, W. Giriat, H. Szynczak, and R. Kowalczyk Phys. Status Solidi B **49**, 71 (1972).
[15]M. Zigone, H. Roux-Buisson, H. Tuffigo, N. Magnea, and H. Mariette, Semicond. Sci. Technol. **6**, 454 (1991).
[16]M. Prakash, M. Chandrasekhar, H. R. Chandrasekhar, I. Miotkowski, and A. K. Ramdas, Phys. Rev. B **42**, 3586 (1990).
[17]D. L. Camphausen, G. A. N. Connel, and W. Paul, Phys. Rev. Lett. **26**, 184 (1971).
[18]J. Allègre, B. Gil, J. Calatayud, and H. Mathieu, J. Cryst. Growth **101**, 603 (1990).
[19]D. Bertho, D. Boiron, A. Simon, C. Jouanin, and C. Priester, Phys. Rev. B **44**, 6118 (1991).
[20]B. Gil, D. J. Dunstan, J. Calatayud, H. Mathieu, and J. P. Faurie, Phys. Rev. B **40**, 5522 (1989).
[21]H. Mathieu, J. Allègre, and B. Gil, Phys. Rev. B **43**, 2218 (1991).
[22]J. Allègre, J. Calatayud, B. Gil, H. Mathieu, H. Tuffigo, G. Lentz, N. Magnea, and H. Mariette, Phys. Rev. B **41**, 8195 (1990).
[23]G. Lentz, A. Ponchet, N. Magnea, and H. Mariette, Appl. Phys. Lett. **55**, 2733 (1989).
[24]A. Ponchet, G. Lentz, H. Tuffigo, N. Magnea, H. Mariette, and P. Gentile, J. Appl. Phys. **68**, 6229 (1990).
[25]R. Zachai, K. Eberl, G. Abstreiter, E. Kasper, and H. Kibbel, Phys. Rev. Lett. **64**, 1055 (1990), and references cited therein.
[26]H. Tuffigo, R. T. Cox, F. Dal'bo, G. Lentz, N. Magnea, H. Mariette, and C. Grattepain, Superlatt. Microstruct. **5**, 83 (1989).
[27]Y. Merle d'Aubigné, Le Si Dang, F. Dal'bo, G. Lentz, N. Magnea, and H. Mariette, Superlatt. Microstruct. **5**, 567 (1989).
[28]M. Matsuura and Y. Shinozuka, Phys. Rev. B **38**, 9830 (1988).
[29]Ph. Peyla, Y. Merle D'Aubigné, A. Wasiela, R. Romestain, H. Mariette, M. D. Sturge, N. Magnéa, and H. Tuffigo, Phys. Rev. B **46**, 1557 (1992).
[30]H. Mariette, F. Dal'bo, N. Magnea, G. Lentz, and H. Tuffigo, Phys. Rev. B **38**, 12443 (1989).
[31]E. Deleporte, G. Peter, J. M. Berroir, and C. Delalande, Surf. Sci. **267**, 137 (1992).
[32]C. G. Van de Walle, Phys. Rev. B **39**, 1871 (1989).